Available online at www.sciencedirect.com

SciVerse ScienceDirect

Ceramics International 39 (2013) 6583–6589

CERAMICS INTERNATIONAL

www.elsevier.com/locate/ceramint

Photocatalytic performance of Pr/In/Nd composite oxides synthesized by solid state reaction

Huiquan Li, Yumin Cui*, Wenshan Hong, Suhua Fan, Liangjun Zhu

School of Chemistry and Chemical Engineering, Fuyang Normal College, Fuyang 236037, People's Republic of China

Received 30 December 2012; received in revised form 24 January 2013; accepted 25 January 2013
Available online 1 February 2013

Abstract

Pr/In/Nd composite oxides with different Pr/In/Nd ratios were successfully prepared using a simple solid state reaction at 873 K. The composites were characterized by X-ray diffraction (XRD), Brunauer–Emmett–Teller (BET) surface area measurements, photoluminescence (PL) spectra and UV–vis diffuse reflection spectroscopy (UV–vis DRS). The photocatalytic activity of Pr/In/Nd composite oxides was investigated by the degradation of methyl orange (MO) in an aqueous solution under UV and visible light irradiation. It is found that compared with pure In_2O_3, the absorption intensity of the Pr/In/Nd composite oxide (Pr/In/Nd = 1:8:1) increases in the 200–800 nm light region and the absorption edge has a shift to longer wavelength. In addition, the Pr/In/Nd composite oxide (Pr/In/Nd = 1:8:1) shows higher UV and visible light photocatalytic activities than pure In_2O_3. The remarkably enhanced photocatalytic activities could be mainly attributed to the fact that proper introduction of Pr_2O_3 and Nd_2O_5 increased the BET surface area of In_2O_3, improved the separation efficiency of photogenerated electrons and holes, and enhanced the absorption intensity in 200–800 nm light region. The effect of various radical scavengers on the degradation of MO showed that $^{\bullet}OH$, $^{\bullet}O_2^-$, h^+ and H_2O_2, especially $^{\bullet}O_2^-$, jointly dominated the photodegradation process of MO under UV light irradiation.

Keywords: Solid state reaction; Composite oxides; Photocatalysis; Methyl orange

1. Introduction

TiO_2-based nanomaterials have been a very attractive research topic and many works have been carried out [1–5]. However, TiO_2 only responds to the UV light ($\lambda < 400$ nm) accounting for ~4% of the solar energy and suffers from the high recombination of photogenerated electron–hole pairs. Therefore, it is very urgent to develop new efficient non-titania photocatalysts. Relevant research in this field has become one of the hot topics in recent years [6–9].

In_2O_3 semiconductor has drawn extensive interest of researchers owing to its great potential applications in sensor modules, photocatalysis, solar cells and transparent electrode materials [10–15], and its composite oxides have been used as photocatalytic hydrogen evolution [16–18]. Pr_2O_3 and Nd_2O_5 have been attractive oxides for scientists due to their thermodynamic stability, high dielectric constant and excellent electrical properties [19–21]. It is well known that the coupling of different semiconductors in composite oxides can transfer electrons from one semiconductor to another semiconductor. This favors the separation of photogenerated electrons and holes and thus improved the photocatalytic efficiency of composite oxides dramatically. However, to the best of our knowledge, there was no report on the synthesis and photocatalytic performance of the Pr/In/Nd composite oxides system.

In this work, Pr/In/Nd composite oxides were successfully synthesized by a simple solid state reaction at 873 K. Various characterization techniques such as XRD, BET, PL and UV–vis DRS were employed to describe the structure and physicochemical properties of Pr/In/Nd composite oxides. The effect of Pr/In/Nd ratios on the photocatalytic activity of Pr/In/Nd composite oxides was investigated in detail. The results showed that the photocatalytic activity of the Pr/In/Nd

*Corresponding author. Tel.: +86 558 2596249; fax: +86 558 2596703.
E-mail address: cuiyumin0908@163.com (Y. Cui).

0272-8842/$ - see front matter © 2013 Elsevier Ltd and Techna Group S.r.l. All rights reserved.
http://dx.doi.org/10.1016/j.ceramint.2013.01.093

composite oxide (Pr/In/Nd = 1:8:1) was greatly enhanced as compared to pure In_2O_3 sample under UV and visible light irradiation.

2. Experimental section

2.1. Catalyst preparation

All reagents are of analytical purity. Pr/In/Nd composite oxides were prepared by the solid state reaction. A typical synthetic procedure toward the Pr/In/Nd composite oxides with different Pr/In/Nd ratios can be described briefly as follows: In_2O_3 (AR, 99.0%, Sinopharm Chemical Reagent Co., Ltd.), Pr_2O_3 (AR, 99.9%, Aladdin) and Nd_2O_5 (3 N, 99.0%, Sinopharm Chemical Reagent Co., Ltd.) were used as the starting raw materials and dried at 673 K. The three kinds of raw materials were mixed uniformly in stoichiometric proportions in acetone, dried at 393 K and crushed in round cakes. Then the mixed oxides were placed in a ceramic boat at 873 K and calcined for 1 h. Pr/In/Nd composite oxides with different weight ratios of Pr/In/Nd of 0:1:0, 1:1:0, 0:1:1, 1:4:1 and 1:8:1 were obtained.

2.2. Characterization

X-ray diffraction (XRD) was performed on a Philips X′pert diffractometer equipped with a Ni-filtered Cu Kα radiation source (λ=0.15418 nm) at a scanning speed of $2^\circ\ min^{-1}$ from 20° to 60°. The X-ray tube was operated at 40 kV and 40 mA. The BET surface areas of samples were determined from N_2 adsorption isotherms at 77 K using a Micromeritics ASAP 2020 instrument with a computer-controlled measurement system. Prior to analysis, 0.1 g samples were degassed at 250 °C and 10 mmHg. The photoluminescence (PL) spectra, obtained at room temperature with an excitation wavelength of 320 nm, were recorded on a CARY Eclipse (America) fluorescence spectrophotometer. UV–vis diffuse reflectance spectra (UV–vis DRS) of the catalysts were determined with a Shimadzu UV-3600 spectrophotometer using $BaSO_4$ as a reference.

2.3. Photocatalytic measurements

The photocatalytic activity of Pr/In/Nd composite oxides was investigated by the degradation of methyl orange (MO) in an aqueous solution. The UV light was obtained by a 300-W high-pressure mercury lamp with an intensity of 15.0 mW cm^{-2} (λ_{max} = 365 nm). The visible light source was a 400-W metal halide lamp (λ_{max} = 588 nm, the visible light intensity of 8.0 mW cm^{-2} and the UV light intensity of 0.7 mW cm^{-2}) with the combination of a cut-off filter ($\lambda > 400$ nm) to eliminate UV radiation during visible light experiments. For each UV light test, 40 mL MO aqueous solution (3.82×10^{-6} mol L^{-1}) and 0.05 g samples were used, while for each visible light test, 40 mL MO aqueous solution (3.82×10^{-6} mol L^{-1}) and 0.50 g samples were used. A general procedure was carried out as follows. First, the MO aqueous solution was placed into a water-jacketed reactor maintained at 298 K, and then the samples were suspended in the solution. The suspension was stirred vigorously for 1 h in the dark to establish the adsorption–desorption equilibrium of MO, then irradiated under UV or visible light for 1 h. About 2.5 mL solution was withdrawn from the reactor and centrifuged and analyzed for the degradation of MO using a TU-1901 spectrophotometer. MO has a maximum absorbance at 464 nm, which was used as a value for monitoring MO degradation. The absorbance was converted to the MO concentration in accordance with a standard curve showing a linear relationship between the concentration and the absorbance at this wavelength.

The degree of mineralization was followed by measuring the total organic carbon (TOC) content in the degraded solution, which was tested by an automated total organic carbon analyzer (TOC-V, Shimadzu, Japan).

In order to study the effects of relevant reactive species, a quantity of different appropriate species quenchers was introduced into the photocatalytic degradation process of MO in a manner similar to the photodegradation experiment. The doses of these species quenchers were referred to the previous literatures [8,22].

2.4. Circle use of catalysts

The cleaned Pr/In/Nd composite oxides were immersed in ethanol for 5 h and rinsed with deionized water, and then dried at 373 K. After this the cleaned Pr/In/Nd composite oxides were reused for removal of the MO dye, and the experiment has been repeated several times.

3. Results and discussion

3.1. Mineralogical composition

Fig. 1 shows the XRD patterns of Pr/In/Nd composite oxides with different Pr/In/Nd ratios. It can be seen that diffraction peaks with 2θ values of 21.5°, 30.56°, 35.5°, 37.7°, 41.8°, 45.6°, 49.3°, 51.9°, 52.8°, 55.9° and 59.2° appear, which can be perfectly indexed to the (211), (222), (400), (411), (332), (134), (521), (440), (433), (611) and (541) crystal planes of In_2O_3 crystalline phase (JCPDS 71-2194), respectively. No characteristic peaks for impurity, such as In or $In(OH)_3$ are observed. The peak of Pr/In/Nd composite oxides around 2θ of 28.8° was indexed to the (002) crystal plane of Pr and the peaks of Pr/In/Nd composite oxides around 2θ of 26.8°, 29.8°, 30.7°, 40.4° and 53.5° were indexed to the (100), (002), (011), (012) and (103) crystal planes of Nd, respectively. The crystallite size of Pr/In/Nd composite oxides was determined according to the Debye–Scherrer equation [23]: $D = K\lambda/\beta \cos\theta$, where λ is the wavelength of the X-ray radiation (λ=0.15418 nm), K is the Scherrer constant (K=0.9), θ is the angle of characteristic X-ray diffraction peak and β is the full-width-at-half-maximum. The relative average crystallite sizes of Pr/In/Nd composite oxides were calculated along

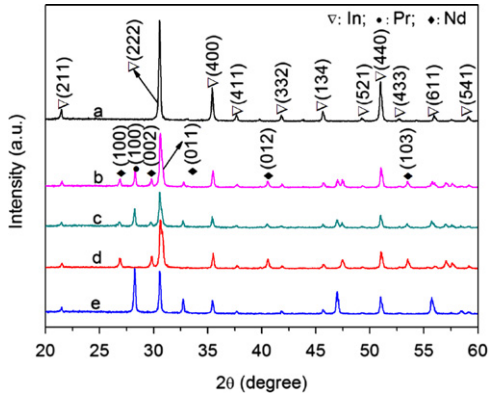

Fig. 1. XRD patterns of Pr/In/Nd composite oxides with different Pr/In/Nd ratios: (a) 0:1:0, (b) 1:8:1, (c) 1:4:1, (d) 0:1:1, and (e) 1:1:0.

the (222) crystallographic direction, and the results are listed in Table 1.

The BET surface areas of the Pr/In/Nd composite oxides with different Pr/In/Nd ratios are indicated in Table 1. It can be seen that the ternary or binary oxide powders have an enhanced surface area in comparison with the pure oxides, which is consistent with the decreasing average crystallite size in the composites.

3.2. Adsorption studies

The photocatalysis performance has been significantly dependent on the adsorbability of photocatalysts [24]. Therefore, a study of MO adsorption was performed on In_2O_3 and Pr/In/Nd composite oxide (Pr/In/Nd = 1:8:1) using 20 mg of catalyst at room temperature in the dark. The adsorption capacity of In_2O_3 and Pr/In/Nd composite oxide (Pr/In/Nd = 1:8:1) is displayed in Fig. 2, in which the adsorption behaviors of MO on In_2O_3 and Pr/In/Nd composite oxide (Pr/In/Nd = 1:8:1) follow the Langmuir model. It can be seen that MO uptake capacity moderately increases in the presence of the Pr/In/Nd composite oxide (Pr/In/Nd = 1:8:1) compared to that of pure In_2O_3 catalyst. The adsorbed quantities of MO, q_t (mg $g^{-1}_{catalyst}$), at time t are calculated according to

$$q_t = [(C_0 - C_t) \times 1000 \times M_W \times V_0]/w_{catalyst} \quad (1)$$

where C_0 and C_t (mol L^{-1}) are the initial concentration and the concentration at time t of MO, respectively; M_W is the molecular weight of MO (g mol^{-1}); V_0 is the volume of MO aqueous solution (L); and $w_{catalyst}$ is the mass of catalyst (g). The equilibrium adsorption capacity (q_e) is usually estimated by the pseudo-first-order and pseudo-second-order model, and the correct values are chosen according to the higher correlation coefficient R^2 [25,26]. Herein, the equilibrium adsorption capacity (q_e) of In_2O_3 and Pr/In/Nd composite oxide (Pr/In/Nd = 1:8:1) is 6.16 and 8.35 mg $g^{-1}_{catalyst}$, respectively. It is obvious that the adsorption ability of pure In_2O_3 catalyst is enhanced by the introduction of Pr_2O_3 and Nd_2O_5, which is a prequisite for good photocatalytic activity [27,28].

Table 1
Textural properties of Pr/In/Nd composite oxides with different Pr/In/Nd ratios.

Pr/In/Nd	Average crystallite sizes (nm)	BET surface areas ($m^2\ g^{-1}$)
0:1:0	32.6	9.20
1:8:1	30.2	13.7
1:4:1	27.1	15.4
0:1:1	22.0	13.2
1:1:0	31.8	11.5

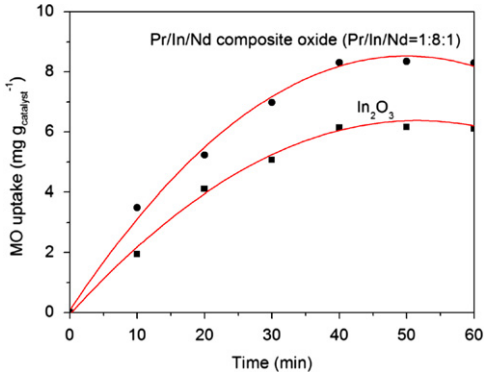

Fig. 2. MO adsorptivity plot for In_2O_3 and Pr/In/Nd composite oxide (Pr/In/Nd = 1:8:1).

3.3. Photocatalytic activity

The effect of Pr/In/Nd ratios on the photocatalytic activity of Pr/In/Nd composite oxides was investigated by degradation of MO in an aqueous solution under UV and visible light irradiation. Fig. 3 shows the UV and visible light photocatalytic activity of Pr/In/Nd composite oxides with different Pr/In/Nd ratios. The results showed that under UV and visible light irradiation the self-degradation of MO solution over a period of 1 h was negligible in the absence of a photocatalyst. However, in the presence of photocatalysts, the irradiation of UV and visible light could result in the obvious degradation of MO, and the Pr/In/Nd ratio in Pr/In/Nd composite oxides exerted great influences on the photocatalytic activity of Pr/In/Nd composite oxides. Compared with pure In_2O_3, the Pr/In/Nd composite oxide (Pr/In/Nd = 1:8:1) obviously presented a higher UV and visible light photocatalytic activity. Moreover, the Pr/In/Nd composite oxide (Pr/In/Nd = 1:8:1) exhibits much higher visible light photoactivity than anatase TiO_2 (UV100, Hombikat, BET: 285 $m^2\ g^{-1}$ crystallite sizes: 1.7 nm), and its UV light photoactivity is slightly lower than that of anatase TiO_2, indicating that proper introduction of Pr_2O_3 and Nd_2O_5 remarkably enhanced the photocatalytic activity of pure In_2O_3.

The UV–vis spectra of MO aqueous solution as a function of UV light irradiation time in the presence of In_2O_3 and Pr/In/Nd composite oxide (Pr/In/Nd = 1:8:1) are illustrated in Fig. 4. It can be seen that the visible region peak intensities in the photodegradation of MO by the Pr/In/Nd composite oxide (Pr/In/Nd = 1:8:1) decrease more obviously than those

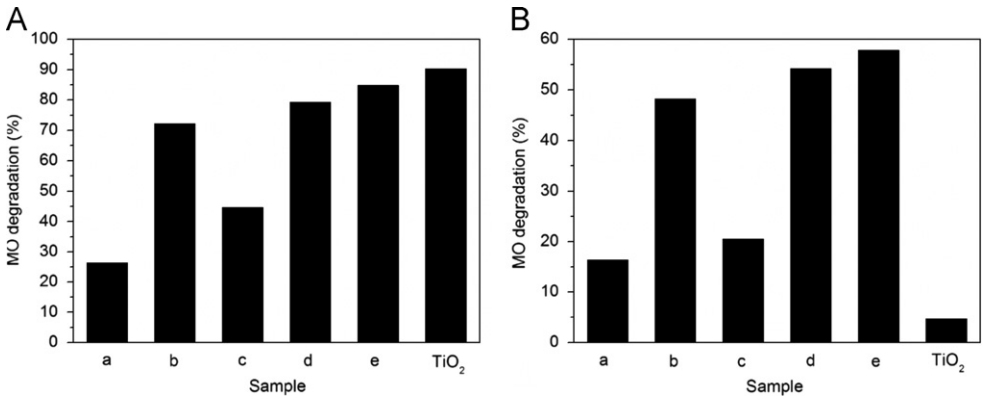

Fig. 3. Effects of Pr/In/Nd ratios in the Pr/In/Nd composite oxides on the degradation of MO under UV (A) and visible (B) light irradiation: (a) 0:1:0, (b) 1:1:0, (c) 0:1:1, (d) 1:4:1, and (e) 1:8:1.

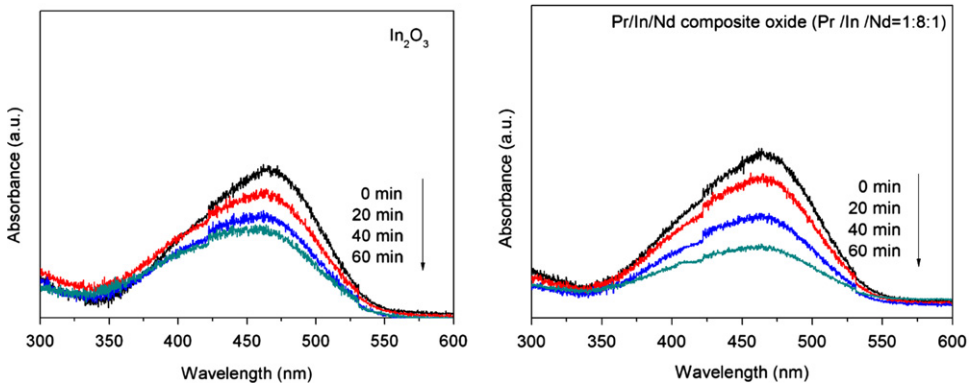

Fig. 4. UV–vis spectra of the MO aqueous solution under UV light irradiation in the presence of In_2O_3 and Pr/In/Nd composite oxide (Pr/In/Nd=1:8:1).

of pure In_2O_3 catalyst after 60 min UV light irradiation, which is in agreement with the results shown in Fig. 3. Since no new peak appears, the loss of absorbance can be mainly attributed to the degradation reaction.

To determine the degree of mineralization of the degraded MO, TOC analysis was also carried out for the reaction in the presence of the Pr/In/Nd composite oxide (Pr/In/Nd=1:8:1). The results are shown in Fig. 5. It can be seen that the TOC value of the MO solution is decreased by approximately 35.2% and 12.6% under UV and visible light irradiation for 100 min, respectively, indicating that the MO molecules can be also mineralized by the Pr/In/Nd composite oxide (Pr/In/Nd=1:8:1).

To test the stability of the photocatalytic performance of the Pr/In/Nd composite oxide (Pr/In/Nd=1:8:1), the circulating runs in the photocatalytic degradation of MO in the presence of the Pr/In/Nd composite oxide (Pr/In/Nd=1:8:1) under UV and visible-light ($\lambda > 400$ nm) were checked (Fig. 6). It can be seen that the photocatalytic activity does not exhibit any significant loss after five recycles for the photodegradation of MO. It indicates that the Pr/In/Nd composite oxide (Pr/In/Nd=1:8:1) has high stability and does not photocorrode during the photocatalytic oxidation of the MO pollutant molecules, which is especially important for its application in the future.

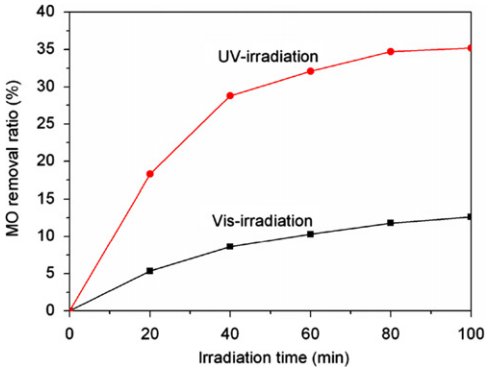

Fig. 5. TOC removal from MO aqueous solution treated with the Pr/In/Nd composite oxide (Pr/In/Nd=1:8:1) under UV and visible light irradiation.

3.4. Light absorption

The UV–vis diffuse reflectance spectra of In_2O_3 and Pr/In/Nd composite oxide (Pr/In/Nd=1:8:1) are shown in Fig. 7. It can be seen that compared with pure In_2O_3, the absorption intensity of Pr/In/Nd composite oxide (Pr/In/Nd=1:8:1) increases in the 200–800 nm region and the absorption edge has a shift to longer wavelength. Thus the

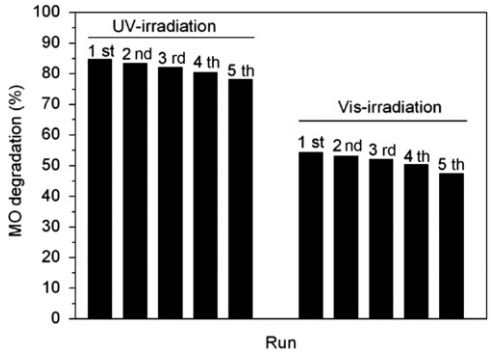

Fig. 6. Photocatalytic degradation of MO in the presence of Pr/In/Nd composite oxide (Pr/In/Nd = 1:8:1) by cycling runs.

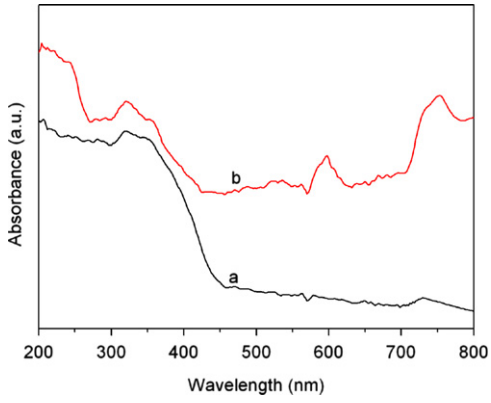

Fig. 7. UV–vis diffuse reflectance spectra of In_2O_3 and Pr/In/Nd composite oxide (Pr/In/Nd = 1:8:1): (a) In_2O_3 and (b) Pr/In/Nd composite oxide (Pr/In/Nd = 1:8:1).

Pr/In/Nd composite oxide (Pr/In/Nd = 1:8:1) shows a higher photocatalytic activity than pure In_2O_3 under UV and visible light irradiation.

3.5. PL properties

The photoluminescence (PL) emission spectra have been widely used to study the recombination rate of photogenerated electron–hole pairs in semiconductors [29]. The comparison of PL emission spectra (excited at 320 nm) of pure In_2O_3 and Pr/In/Nd composite oxide (Pr/In/Nd = 1:8:1) recorded at room temperature is shown in Fig. 8. It can be seen that the two samples have a broad emission peak in the wavelength range of 360–720 nm. The strongest emitting peaks around 469 nm are similar while PL emission intensity of the Pr/In/Nd composite oxide (Pr/In/Nd = 1:8:1) is lower than that of pure In_2O_3, indicating that the recombination of photogenerated charge carriers can be greatly inhibited in the Pr/In/Nd composite oxide (Pr/In/Nd = 1:8:1). That is to say, proper introduction of Pr_2O_3 and Nd_2O_5 in In_2O_3 is beneficial to separate the photogenerated charge carriers and increase the lifetime of charge carriers, and then improve the photocatalytic performance of Pr/In/Nd composite oxides.

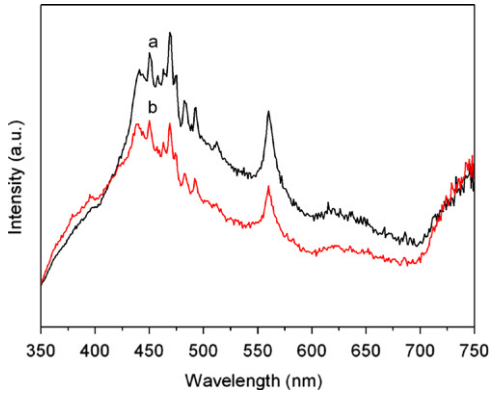

Fig. 8. PL spectra of In_2O_3 and Pr/In/Nd composite oxide (Pr/In/Nd = 1:8:1) recorded at room temperature with the excitation wavelength of 320 nm: (a) In_2O_3, and (b) Pr/In/Nd composite oxide (Pr/In/Nd = 1:8:1).

3.6. Degradation mechanism of MO

The effect of various radical scavengers on the degradation of MO over the Pr/In/Nd composite oxide (Pr/In/Nd = 1:8:1) under UV light irradiation was performed to investigate the underlying photodegradation mechanism. As an $^{\bullet}O_2^-$ scavenger, benzoquinone (BQ) [8] was added to the reaction system, and isopropanol (IPA) [8,9] was introduced as the scavenger of $^{\bullet}OH$. In order to study the role of h^+ and H_2O_2 radical species, ammonium oxalate (AO) [30] and catalase (CAT) [8] were also added to the reaction system, respectively. The results of degradation ratio were expected to be decreased greatly. In Fig. 9, it can be seen that the degradation ratio of MO decreased significantly after the addition of IPA, BQ, AO and CAT. In other words, $^{\bullet}OH$, $^{\bullet}O_2^-$, h^+ and H_2O_2, especially $^{\bullet}O_2^-$, jointly dominated the photodegradation process of MO.

Taking the kinds of reactive species involved in the MO degradation into account, the photocatalytic process could be described as the following:

$$\text{Catalyst} + h\upsilon \rightarrow e^- + h^+ \quad (2)$$

$$e^- + O_2 \rightarrow {}^{\bullet}O_2^- \quad (3)$$

$$e^- + {}^{\bullet}O_2^- + 2H^+ \rightarrow H_2O_2 \quad (4)$$

$$H_2O_2 + e^- \rightarrow {}^{\bullet}OH + OH^- \quad (5)$$

$$H_2O + h^+ \rightarrow {}^{\bullet}OH + H^+ \quad (6)$$

$$OH^- + h^+ \rightarrow {}^{\bullet}OH \quad (7)$$

$$MO + {}^{\bullet}OH \rightarrow \text{products} \quad (8)$$

$$MO + {}^{\bullet}O_2^- \rightarrow \text{products} \quad (9)$$

$$MO + H_2O_2 \rightarrow \text{products} \quad (10)$$

$$MO + h^+ \rightarrow \text{products} \quad (11)$$

In the above process, electron–hole pairs were directly produced by the catalyst after illumination. Then, the photogenerated electrons transferred to CB bottom of the catalyst

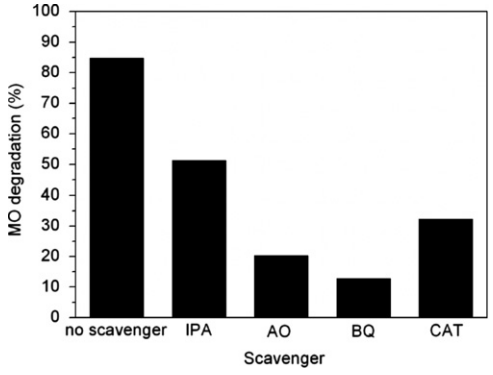

Fig. 9. Effects of different scavengers on the degradation of MO over the Pr/In/Nd composite oxide (Pr/In/Nd = 1:8:1) under UV light irradiation.

and reacted with the adsorbed O_2 on the surface of catalyst to form $^{\bullet}O_2^-$, H_2O_2, and $^{\bullet}OH$, meanwhile, the holes were left on the VB top, reacting with the adsorbed H_2O and OH^- on the surface of catalyst to form $^{\bullet}OH$. $^{\bullet}OH$, $^{\bullet}O_2^-$ and H_2O_2 that could oxidize MO, or the holes reacted directly with MO.

4. Conclusions

In summary, Pr/In/Nd composite oxides were successfully synthesized by a simple solid state reaction at 873 K. Compared with pure In_2O_3, the absorption intensity of the Pr/In/Nd composite oxide (Pr/In/Nd = 1:8:1) increases in the 200–800 nm light region and the absorption edge has a shift to longer wavelength. The Pr/In/Nd ratio exerted great influences on the photocatalytic activity of Pr/In/Nd composite oxides. The Pr/In/Nd composite oxide (Pr/In/Nd = 1:8:1) has the highest photocatalytic performance in all samples under UV and visible light irradiation. The greatly enhanced photocatalytic performance can be mainly attributed to the fact that proper introduction of Pr_2O_3 and Nd_2O_5 increased the BET surface area of pure In_2O_3, improved the separation efficiency of photogenerated electrons and holes, and enhanced the absorption intensity in the 200–800 nm light region. The effect of various radical scavengers on the degradation of MO showed that $^{\bullet}OH$, $^{\bullet}O_2^-$, h^+ and H_2O_2, especially $^{\bullet}O_2^-$, jointly dominated the photodegradation process of MO under UV light irradiation.

Acknowledgment

This work was supported by the National Natural Science Foundation of China (21201037), the Natural Science Foundation of Higher Education Institutions in Anhui Province (KJ2012A217) and school-level item (2012HJJC01ZD) of the Anhui Provincial Key Laboratory for Degradation and Monitoring of Pollution of the Environment.

References

[1] X.B. Chen, L. Liu, P.Y. Yu, S.S. Mao, Increasing solar absorption for photocatalysis with black hydrogenated titanium dioxide nanocrystals, Science 331 (2011) 746–750.

[2] J.N. Schrauben, R. Hayoun, C.N. Valdez, M. Braten, L. Fridley, J.M. Mayer, Titanium and zinc oxide nanoparticles are proton-coupled electron transfer agents, Science 336 (2012) 1298–1301.

[3] S.J. Tan, Y.F. Ji, Y. Zhao, A.D. Zhao, B. Wang, J.L. Yang, J.G. Hou, Molecular oxygen adsorption behaviors on the rutile $TiO_2(110)$-1×1 surface: an in situ study with low-temperature scanning tunneling microscopy, Journal of the American Chemical Society 113 (2011) 2002–2009.

[4] T. Oncescu, M.I. Stefan, P. Oancea, Photocatalytic degradation of dichlorvos in aqueous TiO_2 suspensions, Environmental Science and Technology 17 (2010) 1158–1166.

[5] V. Petrovič, V. Ducman, S.D. Škapin, Determination of the photocatalytic efficiency of TiO_2 coatings on ceramic tiles by monitoring the photodegradation of organic dyes, Ceramics International 28 (2012) 1611–1616.

[6] L.W. Zhang, Y.J. Wang, H.Y. Cheng, W.Q. Yao, Y.F. Zhu, Synthesis of Bi_2WO_6 porous thin films as efficient visible-active photocatalyst, Advanced Materials 21 (2009) 1286–1290.

[7] Y.Z. Li, X. Zhou, X.L. Hu, X.J. Zhao, P.F. Fang, Formation of surface complex leading to efficient visible photocatalytic activity and improvement of photostabilty of ZnO, Journal of Physical Chemistry C 113 (2009) 16188–16192.

[8] G.T. Li, K.H. Wong, X.W. Zhang, C. Hu, J.C. Yu, R.C.Y. Chan, P.K. Wong, Degradation of acid orange 7 using magnetic AgBr under visible light: the roles of oxidizing species, Chemosphere 76 (2009) 1185–1191.

[9] L.S. Zhang, K.H. Wong, H.Y. Yip, C. Hu, J.C. Yu, C.Y. Chan, P.K. Wong, Effective photocatalytic disinfection of *E. coli* K-12 using AgBr–Ag–Bi_2WO_6 nanojunction system irradiated by visible light: the role of diffusing hydroxyl radicals, Environmental Science and Technology 44 (2010) 1392–1398.

[10] Z.M. Li, P.Y. Zhang, T. Shao, X.Y. Li, In_2O_3 nanoporous nanosphere: a highly efficient photocatalyst for decomposition of perfluorooctanoic acid, Applied Catalysis B 125 (2012) 350–357.

[11] I. Hamburg, C.G. Granqvist, Evaporated Sn-doped In_2O_3 films: basic optical properties and applications to energy-efficient windows, Journal of Applied Physics 60 (1986) 123–160.

[12] X. Li, M.W. Wanlass, T.A. Gessert, K.A. Emery, T. Coutts, High-efficiency indium tin oxide/indium phosphide solar cells, Applied Physics Letter 54 (1989) 2674–2676.

[13] D.G. Shchukin, J.H. Schattka, M. Antonietti, R.A. Caruso, Photocatalytic properties of porous metal oxide networks formed by nanoparticle infiltration in a polymer gel template, Journal of Physical Chemistry B 107 (2003) 952–957.

[14] J. Lv, T. Kako, Z. Li, Z. Zou, J. Ye, Synthesis and photocatalytic activities of $NaNbO_3$ rods modified by In_2O_3 nanoparticles, Journal of Physical Chemistry C 114 (2010) 6157–6162.

[15] J. Mu, B. Chen, M. Zhang, Z. Guo, P. Zhang, Z. Zhang, Y. Sun, C. Shao, Y. Liu, Enhancement of the visible-light photocatalytic activity of In_2O_3–TiO_2 nanofiber heteroarchitectures, ACS Applied Materials and Interfaces 4 (2012) 424–430.

[16] D. Wang, Z. Zou, J. Ye, Photocatalytic water splitting with the Cr-doped $Ba_2In_2O_5/In_2O_3$ composite oxide semiconductors, Chemistry of Materials 17 (2005) 3255–3261.

[17] K.R. Reyes-Gil, E.A. Reyes-García, D. Raftery, Nitrogen-doped In_2O_3 thin film electrodes for photocatalytic water splitting, Journal of Physical Chemistry C 111 (2007) 14579–14588.

[18] N. Arai, N. Saito, H. Nishiyama, Y. Shimodaira, H. Kobayashi, Y. Inoue, K. Sato, Photocatalytic activity for overall water splitting of RuO_2-loaded $Y_xIn_{2-x}O_3$ ($x = 0.9-1.5$), Journal of Physical Chemistry C 112 (2008) 5000–5005.

[19] A. Sakai, S. Sakashita, M. Sakashita, Y. Yasuda, S. Zaima, S. Miyazaki, Praseodymium silicate formed by postdeposition high-temperature annealing, Applied Physics Letters 85 (2004) 5322–5324.

[20] G. Lupina, T. Schroeder, J. Dabrowski, C. Wenger, A.U. Mane, H.J. Mussig, P. Hoffmann, D. Schmeisser, Praseodymium silicate films on Si(100) for gate dielectric applications: physical and electrical characterization, Journal of Applied Physics 99 (2006) 114109–114116.

[21] T.M. Pan, F.J. Tsai, C.I. Hsieh, T.W. Wu, Structural properties and electrical characteristics of praseodymium oxide gate dielectrics, Electrochemical and Solid State Letters 10 (2007) 21–24.
[22] J. Cao, B.Y. Xu, B.D. Luo, H.L. Lin, S.F. Chen, Novel BiOI/BiOBr heterojunction photocatalysts with enhanced visible light photocatalytic properties, Catalysis Communications 13 (2011) 63–68.
[23] M. Galceran, M.C. Pujol, C. Zaldo, F. Díaz, M. Aguiló, Synthesis, structural, and optical properties in monoclinic Er:$KYb(WO_4)_2$ nanocrystals, Journal of Physical Chemistry C 113 (2009) 15497–15506.
[24] S.F. Chen, Y.Z. Liu, Study on the photocatalytic degradation of glyphosate by TiO_2 photocatalyst, Chemosphere 67 (2007) 1010–1017.
[25] W. Kangwansupamonkon, W. Jitbunpot, S. Kiatkamjornwong, Photocatalytic efficiency of TiO_2/poly[acrylamide-co-(acrylic acid)] composite for textile dye degradation, Polymer Degradation and Stability 95 (2010) 1894–1902.
[26] Y.S. Ho, G. McKay, A comparison of chemisorption kinetic models applied to pollutant removal on various sorbents, Transactions of the Institution of Chemical Engineers 76B (1998) 332–340.
[27] H. Zhang, X.J. Lv, Y.M. Li, Y. Wang, J.H. Li, P25-graphene composite as a high performance photocatalyst, ACS Nano 4 (2008) 380–386.
[28] W. Morales, M. Cason, O. Aina, N.R. de Tacconi, K. Rajeshwar, Combustion synthesis and characterization of nanocrystalline WO_3, Journal of the American Chemical Society 130 (2008) 6318–6319.
[29] Y.M. Wu, J.L. Zhang, L. Xiao, F. Chen, Preparation and characterization of TiO_2 photocatalysts by Fe^{3+} doping together with Au deposition for the degradation of organic pollutants, Applied Catalysis B 88 (2009) 525–532.
[30] N. Zhang, S.Q. Liu, X.Z. Fu, Y.J. Xu, Synthesis of M@TiO_2 (M = Au, Pd, Pt) core–shell nanocomposites with tunable photoreactivity, Journal of Physical Chemistry C 115 (2011) 9136–9145.